APPLIED PHYSICS LETTERS **89**, 201110 (2006)

Temperature mapping and thermal lensing in large-mode, high-power laser diodes

P. K. L. Chan[a] and K. P. Pipe
Solid State Thermal Physics Laboratory, University of Michigan, Ann Arbor, Michigan 48109-2025

J. J. Plant, R. B. Swint, and P. W. Juodawlkis
Lincoln Laboratory, Massachusetts Institute of Technology, Lexington, Massachusetts 02420-9108

(Received 1 July 2006; accepted 9 October 2006; published online 16 November 2006)

The authors use high-resolution charge-coupled device based thermoreflectance to derive two dimensional facet temperature maps of a $\lambda = 1.55\ \mu$m InGaAsP/InP watt-class laser that has a large ($>5\times5\ \mu m^2$) fundamental optical mode. Recognizing that temperature rise in the laser will lead to refractive index increase, they use the measured temperature profiles as an input to a finite-element mode solver, predicting bias-dependent spatial mode behavior that agrees well with experimental observations. These results demonstrate the general usefulness of high-resolution thermal imaging for studying spatial mode dynamics in photonic devices. © *2006 American Institute of Physics*. [DOI: 10.1063/1.2388884]

In semiconductor lasers, key parameters such as threshold current, efficiency, and wavelength are closely related to temperature. These dependencies are especially important for high-power lasers, in which device heating is the main cause of decreased performance and failure. Heat sources such as nonradiative recombination in the active region typically cause the temperature to be highly peaked within the device, leading to thermal lensing due to the increase in refractive index with temperature. Such optical mode variation caused by highly nonuniform temperature profiles has previously been studied in vertical-cavity surface-emitting lasers (VCSELs) and antiguided laser diode arrays. In VCSELs without built-in lateral index guiding, the refractive index step induced by a temperature increase generates an artificial thermal lens which can improve optical confinement and thus increase differential efficiency.[1,2] In antiguided diode laser arrays, high index step islands have been demonstrated to reduce thermal lensing.[3]

Here we use high-resolution thermal imaging of a high-power edge emitting laser not only to examine device heating but also to produce a map of thermally induced index changes which lead to both compression and translation of the optical mode. Such alteration of the mode can potentially lead to both decreased efficiency in cases for which the mode moves to a high-loss region of a laser and modified fiber coupling efficiency as the mode changes shape and moves relative to an optical collection aperture.

The device under test [Fig. 1(a)] is a 1-cm-long InGaAsP/InP watt-class slab-coupled optical waveguide laser (SCOWL) having a 4.9-μm-thick InGaAsP waveguide and a 5.7-μm-wide etched ridge. The laser emits at $\lambda = 1.55\ \mu$m and has a threshold current of $I_{th} = 500$ mA,[4] These devices generate large optical modes ($>5\times5\ \mu m^2$) with nearly circular diffraction-limited beam quality by filtering higher-order modes from an otherwise multimode InGaAsP rib waveguide to an adjacent slab region and tailoring the quantum wells (QWs) such that the fundamental mode is the only mode with net gain. In addition to the advantages of high optical power and single mode output, the large circular beam quality makes SCOWL emission suitable for high efficiency butt coupling into optical fibers without the use of lenses.

In order to generate two dimensional (2D) temperature maps of the SCOWL facets with high spatial (500 nm) and temperature (450 mK) resolutions, we employ a thermoreflectance setup using a charge-coupled device (CCD) camera for image acquisition.[5] Better temperature resolution (10 mK) can be achieved with this technique by averaging data over longer experiment times;[6] however, such resolution is not required for this study. Thermoreflectance techniques are based on deriving the temperature increase (ΔT) of a sample surface by measuring the normalized change of surface reflection coefficient ($\Delta R/R$). The temperature variation can be written as $\Delta T = \kappa^{-1}(\Delta R/R)$, where the thermoreflectance coefficient κ depends on the sample material and the illuminating wavelength. In the setup used here, the device to be measured is biased with a sine wave at 10 Hz while λ

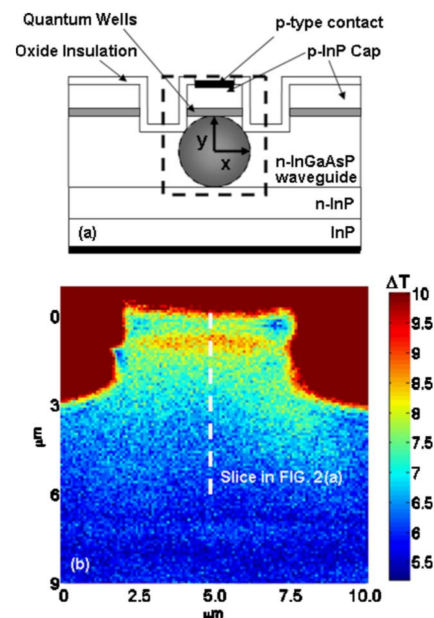

FIG. 1. (Color online) (a) Structure of SCOWL and (b) 2D temperature map of the device at a bias of 2.4 A.

[a]Electronic mail: klchan@umich.edu

 © 2006 American Institute of Physics

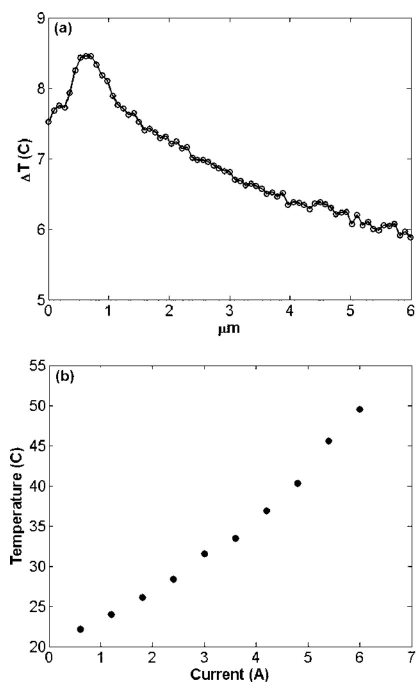

FIG. 2. (a) Vertical cross section of laser temperature at a bias current of 2.4 A, and (b) spatially averaged active region temperature at different bias currents.

=472 nm light-emitting diode (LED) illumination is reflected off of its surface; this reflected light is collected by an objective with a numerical aperture of 0.55 and imaged by a CCD camera operating at a 40 Hz frame rate. A high-pass filter with high optical density (OD6) ensures that no 1.55 μm laser light contaminates the measurement; this is confirmed by thermoreflectance measurements taken without LED illumination that demonstrate no observed signal on the CCD. The four pictures taken by the CCD camera during each bias cycle of the device are combined to calculate $\Delta R/R$ at each pixel, averaging over many device periods.[7] In order to translate $\Delta R/R$ into temperature increase, the thermoreflectance coefficient (κ) must be measured accurately. This calibration is performed by oscillating the temperature of the device heat sink and carrying out a thermoreflectance measurement while using microthermocouples to measure ΔT. The measured thermoreflectance coefficients for InP and InGaAsP are very close to each other with a value of $\kappa = 2.2\times 10^{-4}$ K^{-1}.

The derived temperature map of the SCOWL facet at a bias of 2.4 A is shown in Fig. 1(b), with a cross-sectional slice of the temperature plotted in Fig. 2(a). Significant heating is observed near the active region, and the falloff of temperature toward the 20° C heat sink is also visible. The spatially averaged active region temperature at different current levels is plotted in Fig. 2(b). The continuous temperature increase near the active region with increasing current is most likely due to nonradiative recombination of carriers.[8]

TABLE I. Refractive index parameters used in the finite-element model.

Material	n_r	$\partial n_r/\partial T$	References
InP	3.16	1.9×10^{-4}	13
InGaAsP	3.36	5.0×10^{-4}	14 and 15

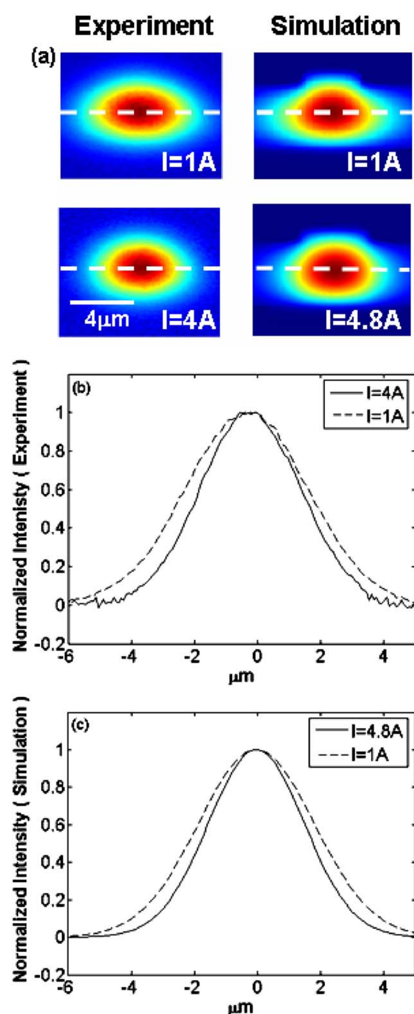

FIG. 3. (Color online) Experiment and simulation results of the optical mode at different bias levels. Cross sections of the normalized experimental and simulation results [dotted lines in Fig. 3(a)] are plotted in Figs. 3(b) and 3(c).

2D temperature maps obtained at different current levels are used as inputs to a finite-element-based optical mode solver to account for the fact that the refractive indices of the laser materials change as the temperature varies. The change of refractive index Δn_r can be written as[9] $\Delta n_r = (\partial n_r/\partial n)\Delta n + (\partial n_r/\partial T)\Delta T$, where n_r is the refractive index, n is the carrier density, and T is the temperature. The first term is the change of refractive index due to carrier density variation, and the second term is the change of refractive index due to temperature variation. It should be pointed out that the variations of carrier density and temperature usually have opposite effects on the refractive index; for most semiconductors, $\partial n_r/\partial n$ has a negative sign while $\partial n_r/\partial T$ has a positive sign.

Thermoreflectance measurements performed at threshold bias (~500 mA) show no $\Delta R/R$ signal, implying that there is no carrier-induced change in index below threshold. While carrier density is expected to clamp above threshold for an ideal laser, carrier leakage in a practical laser can cause variation in carrier density. Measurements of the spontaneous emission spectrum of the SCOWL show that this leakage is minimal even at high bias ($I=6$ A) due to SCOWL's high-barrier carrier blocking layers, indicating that carrier-induced index change above threshold can be neglected as well.

We can estimate the error caused by carrier-induced index change for this thermoreflectance technique when it is

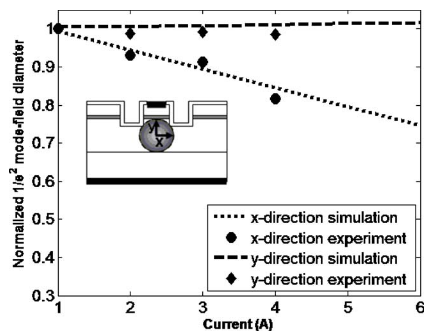

FIG. 4. (Color online) Normalized $1/e^2$ mode-field diameter of the optical mode in the x and y directions. The x direction has an 18% drop as the current increases from 1 to 4 A.

applied in general to common InP-based lasers which do suffer leakage at high bias by examining prior transport models for these devices. These models predict that the majority of the carrier density change occurs in the quantum wells closest to the p cladding.[10] The induced reflectance error can be calculated by $\Delta R=4(n_r-1)/(n_r+1)^3\Delta n_r$; a typical InGaAsP QW high-bias carrier concentration of 2×10^{18} cm^{-3} will yield a refractive index variation Δn_r of -0.02 and $\Delta R/R=-0.008$.[9,11] At $I=6$ A, we measure $\Delta R/R$ to be approximately 0.0058 in the QW region for the SCOWL and use this as a typical value. Accounting for spatial averaging (the QW region is only 40 nm of the 500 nm resolution), this would translate to an error in temperature measurement of 15% for the line of pixels directly on the QWs. It is worth noting that although much less error due to carrier density changes is expected for measurements on the SCOWL because it has very little carrier leakage, if the QW index is varied by -0.02 as a test case, the finite-element optical mode solver shows no significant change in the mode shape, size, or position. This provides further evidence that carrier-induced index changes can be neglected for the study of optical mode dynamics described here.

The quantum-confined Stark effect, which leads to QW reflectance changes due to applied electric field, is likewise neglected here. Reverse-bias measurements at the same magnitude as the forward bias (3.5 V) show no $\Delta R/R$ signal. In addition, the LED illumination at $\lambda=472$ nm has an energy much greater than the QW band gap; the field-induced reflectance change at this wavelength is assumed to be negligible.[12]

As a result of the above assumptions, we focus on thermally induced index change using the values of $\partial n_r/\partial T$ listed in Table I for our simulation. The optical field in the laser is governed by Helmholtz equation $\nabla^2E(x,y)+n_r^2(T)k_0^2E(x,y)=0$, where $k_0=2\pi/\lambda$ and E is the electric field. We use a finite-element model to solve this equation, taking into consideration the index shifts due to the measured temperature profile and plotting the result in Fig. 3.

Optical near-field mode patterns obtained by a phosphor-coated Si CCD camera focused through an attenuator on the facet at $I=1$ and 4 A are shown in Fig. 3 and agree well with the simulated results. At low bias ($I=1$ A), the beam spreads more widely in the InGaAsP waveguide region and is more elliptical. The measured $1/e^2$ mode-field diameters are 7.8 and 5.5 μm in the horizontal (x) and vertical (y) directions [see Fig. 1(a)], respectively. This large mode size is very important to attain high fiber coupling efficiency. At high bias ($I=4$ A), the beam shrinks and becomes more circular and confined in the waveguide region, with measured $1/e^2$ mode-field diameters of 6.4 μm and 5.3 in the x and y directions. This is consistent with thermal lensing, as active region heating causes an increase in refractive index which pulls the mode more into the ridge. The observed improvement in mode circularity at high current should increase the coupling efficiency to circular-mode fibers.

In order to further verify how the mode size is affected by thermal lensing, the normalized $1/e^2$ mode-field diameters of the optical beam in the x and y directions are plotted in Fig. 4. It can be observed that the diameter in the x direction decreases by about 18% as the current increase from 1 to 4A, in contrast to the y direction where no significant change is observed. This is because the index contrast of the thick InGaAsP waveguide dominates thermally induced mode shaping in the y direction, while the much smaller confinement in the x direction ($\Delta n_r/n_r<10^{-3}$) makes it more susceptible to thermal shaping. The model shows good agreement with the measured behavior of the mode.

In conclusion, we have used high-resolution CCD-based thermoreflectance to image heat transfer in a high-power, large-mode edge emitting semiconductor laser. Thermal images were then used as inputs to a finite-element-based mode solver, yielding mode changes due to thermal effects. These mode dynamics were in very good agreement with direct beam pattern measurements. Lateral mode shape was shown to decrease by as much as 18% as the current increases from 1 to 4 A. The CCD-based thermoreflectance technique applied here provides a powerful general technique for studying spatial mode dynamics in photonic devices.

[1]M. Brunner, K. Gulden, R. Hövel, M. Moser, and M. Ilegerms, Appl. Phys. Lett. **76**, 7 (2000).
[2]D. Lüerßen, R. J. Ram, and J. A. Hudgings, CLEO (CLEO, Baltimore, MD, 2005), Vol. 2, pp. 1378–1380.
[3]H. Yang, L. J. Mawst, and D. Botez, Appl. Phys. Lett. **76**, 1219 (2000).
[4]J. J. Plant, P. W. Juodawlkis, R. K. Huang, J. P. Donnelly, L. J. Missaggia, and K. G. Ray, IEEE Photonics Technol. Lett. **17**, 735 (2005).
[5]P. K. L. Chan, K. P. Pipe, Z. Mi, J. Yang, P. Bhattacharya, and D. Lüerßen, Appl. Phys. Lett. **89**, 011110 (2006).
[6]D. Lüerßen, J. A. Hudgings, P. M. Mayer, and R. J. Ram, *21st Annual IEEE Semiconductor Thermal Measurement and Management Symposium* (IEEE, San Jose, 2005), p. 235.
[7]S. Grauby, B. C. Forget, S. Holé, and D. Fournier, Rev. Sci. Instrum. **70**, 3603 (1999).
[8]J. Piprek, K. White, and A. J. SpringThorpe, IEEE J. Quantum Electron. **38**, 1253 (2002).
[9]M. Brunner, K. Gulden, R. Hövel, M. Moser, and M. Ilegems, Appl. Phys. Lett. **76**, 7 (2000).
[10]J. Piprek, P. Abraham, and E. Bowers, Appl. Phys. Lett. **74**, 489 (1999).
[11]G. Schraud, G. Muller, L. Stoll, and U. Wolff, Electron. Lett. **27**, 297 (1991).
[12]S. J. B. Yoo, M. A. Koza, R. Bhat, and C. Caneau, Appl. Phys. Lett. **72**, 3246 (1998).
[13]E. Gini and H. Melchior, J. Appl. Phys. **79**, 4335 (1996).
[14]Y. Shoji, H. Yokoi, and T. Mizumoto, Jpn. J. Appl. Phys., Part 1 **38**, 590 (2004).
[15]H. Tanobe, Y. Kondo, Y. Kadota, Y. K. Okamoto, and Y. Yoshikuni, CLEO/Pacific Rim (CLEO, Chiba, 1997), p. 283.